



# Study on the Mechanical Properties and Microstructure of Fiber-Reinforced Concrete Subjected to Sulfate Erosion

Jianguo Lu<sup>1,2</sup> · Junni Liu<sup>1</sup> · Xiaoyi Fan<sup>1</sup> · Xusheng Wan<sup>1</sup> · Jiajia Gao<sup>3</sup> · Jiacheng Zhang<sup>1</sup> · Pengcheng Li<sup>4</sup>

Received: 13 December 2021 / Accepted: 29 March 2022 / Published online: 9 September 2022  
© King Fahd University of Petroleum & Minerals 2022

## Abstract

It is of great significance to overall evaluate the degree and process of sulfate erosion on concrete, especially for the fiber-reinforced concrete (FRC). This paper investigated the effect of steel fiber (SF), polypropylene fiber (PPF), and basalt fiber (BF) on the mechanical properties and microstructure of concrete exposed to sulfate erosion. The compressive strength, mass change rate, and scanning electron microscope (SEM) images of the steel fiber-reinforced concrete (SFRC), polypropylene fiber-reinforced concrete (PPFRC), and basalt fiber-reinforced concrete (BFRC) were obtained. The results revealed that the sodium solution concentration affected the compressive strength and relative elasticity modulus of concrete, the compressive strength and relative elasticity modulus diminished with the erosion concentration increased. Further, for the FRC, there was an optimum fiber content for the compressive strength of concretes to resist sulfate erosion, whereby the optimum fiber contents for the SFRC, PPFRC, and BFRC were 3.0%, 1.0‰ and 0.5‰, respectively. Moreover, the mass change rates for the PPFRC were lower than those for the BFRC, while being higher than those for the SFRC. The mass change rate of PPFRC exposed to sulfate erosion concentrations of 3%, 5% and 7% could be divided into three stages, i.e., decreasing stage with the mass change rate below zero, increasing stage with the pores of concretes filling by some expansion products, and declining stage with some mortar peeling out. Additionally, the number and shape of expansion products increased with the erosion age and sulfate solution concentration, together with the depth and width of cracks in concrete.

**Keywords** Steel fiber · Polypropylene fiber · Basalt fiber · Mechanical properties · Microstructure · Sulfate erosion

## 1 Introduction

Concrete is a multiphase compound bonded by water, fine aggregate, coarse aggregate, and cement, which is widely used in practical engineering applications, e.g., buildings, dams, roads, and bridges. However, due to the low tensile strength, poor impact toughness, high brittleness, and poor ductility, the performance of concrete cannot meet the

structure requirement and expected service life [1]. With the development of civil engineering, more attention has been paid to the durability of structure. At the same time, higher strength of concrete is demanded. It has been confirmed that the inherent deficiencies of concrete can be significantly improved by added discontinuous chopped fibers into concrete [2, 3]. Generally, fibers could be divided into two categories according to the elastic modulus, namely, the rigid fibers (e.g., glass fibers, basalt fibers, and steel fibers) and flexible fibers (e.g., nylon fibers, polypropylene fibers, and some natural fibers), in which steel fiber (SF) and polypropylene fiber (PPF) are the two superior reinforced materials because of low cost. Also, basalt fiber (BF) is another well-behaved fiber due to high mechanical strength [4, 5], high heat and chemical resistance [6], high temperature stability [7], environmentally friendly and non-hazardous [7–10]. The use of such fibers mixed concretes facilitate the construction processes and is greatly beneficial when the concrete structure is exposed to complicated harsh environments.

✉ Xiaoyi Fan  
fxy@swpu.edu.cn

<sup>1</sup> School of Civil Engineering and Geomatics, Southwest Petroleum University, Chengdu 610513, China

<sup>2</sup> State Key Laboratory of Frozen Soil Engineering, Northwest Institute of Eco-Environment and Resources, Chinese Academy of Sciences, Lanzhou 730000, China

<sup>3</sup> Dean's Office, Southwest Petroleum University, Chengdu 610513, China

<sup>4</sup> Institute of Safety, Environment Protection and Technical Supervision, PetroChina Southwest Oil and Gas Field Company, Chengdu 610041, China



Many studies have been conducted on the improvement effect of fiber on the mechanical properties. Typically, the added fiber into concrete could bridge micro-cracks in concrete matrix and lead stress distribution, thus reducing stress concentration and preventing the stress continuation to spread at the crack points [11, 12], especially in the crack propagation stage. Many studies have shown that the addition of fibers into concrete can significantly enhance the durability and mechanical properties of concrete structure, thereby obtaining high toughness, high strength, and high durability in fiber-reinforced concrete (FRC) [4, 6, 13, 14]. All these can contribute to promote the application field scopes of concrete. Considering the mechanical properties of FRC, many studies have mainly focused on the compressive strength [15–18], flexural strength [16, 18], tensile strength [15, 18], elasticity modulus [16–19], stress–strain behavior [20, 21], creep [22, 23], damping ratio [19], ultra-sonic pulse velocity [18], and drying shrinkage of FRC [24, 25]. It has been verified that the added SF has a positive influence on the compressive strengths of SFRC. For example, the maximum compressive strength of concrete with adding 1.5% SF was 15.3% higher than that without SF addition [15], and the compressive strength and splitting tensile strength of the concrete with the addition of 1% SF and 15% silica fume increased by 17.6% and 13.8% for aspect ratios of 80 and 65, respectively [16]. Yuan et al. [26] investigated the PPF on the mechanical and microstructure of concrete considering the fiber water/cement ratio and found that the water/cement ratio could influence the optimum fiber content. It was also demonstrated that the added BF could also enhance the mechanical strength, while the optimum BF content and the enhancement effect were variable [6, 13, 27].

Further, some fiber parameters, such as volume of fiber inclusion, fiber geometry, fiber type, fiber matrix, and orientation of fiber, can also significantly influence the performances of concretes [14]. The SEM observations revealed that the added fibers can enhance the pore structure of concrete matrix and accumulate on the attached mortar surface, especially the interfacial transition zones, thus improving the strength and ductility of the concrete [6, 27]. As indicated above, it can be seen that the studies on the mechanical properties and microstructure of steel fiber-reinforced concrete (SFRC), polypropylene fiber-reinforced concrete (PPFRC), and basalt fiber-reinforced concrete (BFRC) exposed to sulfate erosion are insufficient. As such, to broaden the practical application of FRC, the mechanical properties and microstructure of FRC are important issues to be addressed.

Saline soils are widely distributed all over the world, with the areas ranging from coastal to inland regions, and humid to desert area [28, 29]. For example, in northwest China (i.e., Qinghai, Gansu, Ningxia, and Xingjiang), there are 69.3% covered with saline soils [30]. Thus, the rich sulfate in soils, ground water, and seawater could not be ignored.

Typically, the damage progress of concrete caused by salt erosion depends on concrete characteristics [31], and salt erosion properties, e.g., composition and concentration of chemical solution [32], temperature [33], moisture [34], and loading conditions [35]. Salt was the main factor causing the concrete erosion, with serious detrimental effects on the service life of concrete structure [36]. The migration processes of saline ions in concrete could be typically regarded as the coupling between the capillary action and concentration gradient [37]. Moreover, the salt erosion progress caused by sodium solution occurs in stages, where the expansion of surface of the sample leads to the formation of crack in the inner part without chemically unaltered at first stage. With increasing immersion, the surface of concrete sample disintegrates, causing the sodium sulfate solution to directly flow into the interior zone and react with hydration products. Simultaneously, the expansive products, e.g., salt crystals, gypsum and ettringite, remain in the regions, and the interior zone becomes the expanding zone. Eventually, further cracking of the interior and penetration channel occurs [38–40]. Huang et al. [41] studied the influential factors (e.g., strength grade, basalt fiber content, fly ash content and aggregate type) on the chloride diffusion process of coral aggregate concrete, and concluded that the free chloride concentration of coral aggregate concrete was far higher than that of ordinary aggregate concrete. Considering the applicability of seawater sea-sand concrete (SWSSC) in island and coastal regions, Han et al. [38] explored the sulfate resistance of SWSSC with high-ferrite Portland cement and verified that this eco-friendly concrete had a good performance on the sulfate resistance. Besides, some other properties of concrete after salt erosion, such as relative dynamic elastic modulus [42], pore structures [43, 44], thermal characteristics [42], and mass loss [43] have also been studied. The above studies show that salt erosion has a significant impact on the concrete durability. However, the mechanism of salt erosion as well as the most unfavorable concentration of the sulfate solution is not clear. Thus, the influence of solution concentrations on the mechanical and microstructure of FRC should be further studied.

Thus, this study investigated the effect of added steel fiber (SF), polypropylene fiber (PPF), and basalt fiber (BF) on the mechanical properties and microstructure of the concrete exposed to sulfate erosion. The compressive strength, coefficient of residual mechanical strength, and relative elasticity modulus of samples were quantitatively analyzed considering the fiber type, fiber content, and concentration of sodium sulfate solution. Furthermore, the mass changes of samples were measured to determine the optimal fiber content and the most unfavorable sulfate solution concentration. Additionally, the microstructure of the samples after 150 days of sulfate erosion was observed to further explore the variations of strength and structure of concretes. These investigations help us better understand the deterioration of mechanical



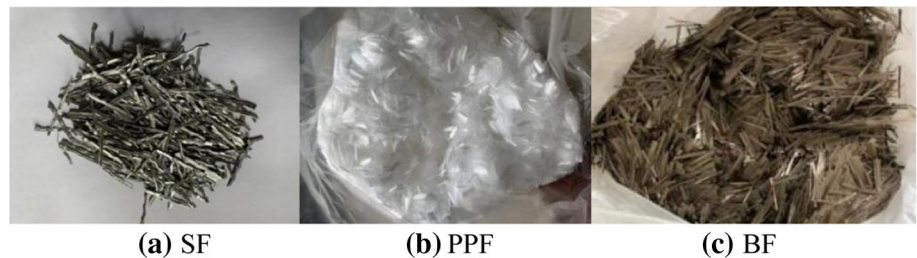
**Table 1** Chemical and mineral composition of cement

Composition	Chemical composition								Mineral composition			
	SiO <sub>2</sub>	Al <sub>2</sub> O <sub>3</sub>	Fe <sub>2</sub> O <sub>3</sub>	CaO	MgO	SO <sub>3</sub>	Na <sub>2</sub> O	K <sub>2</sub> O	C <sub>3</sub> S	C <sub>2</sub> S	C <sub>3</sub> A	C <sub>4</sub> AF
Content (wt.%)	21.04	5.53	3.98	62.32	1.75	2.62	0.46	0.19	53.07	23.19	4.74	11

**Table 2** Physical and mechanical properties of cement

Cement	Specific surface area (m <sup>2</sup> /kg)	Soundness	Ignition loss (%)	Setting time (min)		Compressive strength (MPa)		Flexural strength (MPa)	
				Initial	Final	3 days	28 days	3 days	28 days
				P.O42.5R	366	Qualified	1.21	188	275

**Fig. 1** Fibers used in the experiment



properties and microstructure of FRC exposed to sulfate erosion.

## 2 Experimental Procedure

### 2.1 Raw Materials

P.O42.5R ordinary Portland cement (C), produced by the Lafarge Cement Co., Ltd. in Sichuan Province, was used in the experiment. The chemical and mineral composition of cement is listed in Table 1, and the physical property is listed in Table 2. Natural river sand with a 2.58 fineness modulus, mud content of 1.5%, and apparent density of 2580 kg/m<sup>3</sup> was used as fine aggregate (FA). The coarse aggregate (CA) was employed with a continuous gradation of 5–20 mm in diameter and an apparent density of 2660 kg/m<sup>3</sup>. A polycarboxylate-based superplasticizer (PBS) with a water reducing rate of 25% was also utilized. The tap water (W) in Chengdu area was used in mixing.

Three fibers (i.e., SF, PPF and BF) were used in the experiment. The SF was the sheared wavy type with a diameter of 0.60 mm and a length of 35 mm, which is one of the widely used steel fibers in SFRC. The PPF was a single fiber type with a diameter of 60 μm and a length of 9 mm. The BF was chopped type with 60 μm diameter and 18 mm length. The shape and main properties of the used fibers are shown in Fig. 1 and Table 3, respectively.

### 2.2 Mix Proportions

The detail of all 12 different mixtures are listed in Table 4. Five concentrations of sodium sulfate solution as 0%, 3%, 5%, 7% and 10% were designed, each concentration immersed four group, and each group have three samples. For all samples, the water/cement ratio was 0.4. The fiber content is the ratio of the volume of fiber to that of the concrete matrix. Here, OPC denotes the ordinary concrete without the fiber. The SF1, SF2, and SF4 represent the SFRC with the SF volume fractions of 1.0%, 2.0%, and 4.0%, respectively.

**Table 3** Physical and mechanical properties of the fibers

Types	Length (mm)	Diameter (μm)	Density (g/cm <sup>3</sup> )	Elastic modulus (GPa)	Tensile modulus (GPa)
SF	35	600	7.8	200	1.0
PPF	9	60	0.91	4.1	0.4
BF	18	15	2.56	75	4.5

**Table 4** Mix proportions (kg/m<sup>3</sup>)

Sample	W/C	W	C	CA	FA	Fiber	PBS	Fiber volume fraction
OPC	0.4	161	403	606	1230	–	4	0.0
SF1	0.4	161	403	580	1178	78	4	1.0%
SF2	0.4	161	403	554	1125	156	4	2.0%
SF4	0.4	161	403	503	1021	312	4	4.0%
PP1	0.4	161	402.6	606	1230	0.4	4	1.0%
PP2	0.4	161	402.2	606	1230	0.8	4	2.0%
PP4	0.4	161	401.4	606	1230	1.6	4	4.0%
PP6	0.4	161	400.6	606	1230	2.4	4	6.0%
BF0.5	0.4	161	401	606	1230	1.4	4	0.5%
BF1.0	0.4	161	400	606	1230	2.7	4	1.0%
BF1.5	0.4	161	398	606	1230	4.1	4	1.5%
BF2.0	0.4	161	396	606	1230	5.4	4	2.0%

Similarly, the PP1, PP2, PP4, and PP6 represent the PPFRC with the PPF volume fractions of 1.0%, 2.0%, 4.0% and 6.0%, respectively. Finally, the BF0.5, BF1.0, BF1.5, and BF2.0 denote the BFRC with the BF volume fractions of 0.5%, 1.0%, 1.5% and 2.0%, respectively.

### 2.3 Sample Preparation and Curing

To obtain uniform fiber-reinforced concretes, the schematic diagram of the mixing procedure for fiber-reinforced concretes is shown in Fig. 2. The order of placing raw materials into the forced mixer and the applied stirring time were as follows: (a) the coarse aggregate and fine aggregate were poured into the forced mixer and stirred for around 30 s; (b) the cement was added and stirred for another 30 s; (c) approximately 30% water was added and stirred for around 90 s; (d) fibers and 30% water were added and stirred for another 90 s; (e) a polycarboxylate-based superplasticizer and the remaining water were added and stirred until the mixture was uniform (Fig. 2). Then, a slump test was performed to test the workability of the concrete, and the slump value was 82 mm, which accords with the design of the mixture.

The concrete mixture was casted into 100 mm × 100 mm × 100 mm cubic molds and compacted on the vibration table. Then, the samples were covered with an impervious plastic film to prevent moisture from evaporating and cured in the mold for 24 h. Subsequently, the samples were demolded and placed in a standard curing room at the ambient temperature of 20 ± 2 °C and relative humidity over 95% for 28 days.

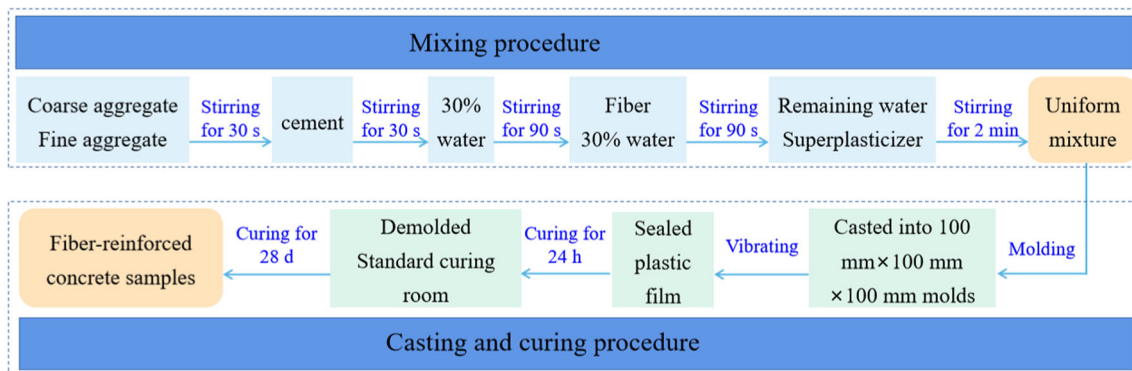
### 2.4 Sulfate Erosion Description

After curing for 28 days, the samples were immersed in 0%, 3%, 5%, 7% and 10% sodium sulfate solutions at room ambient temperature, respectively. The solutions were replaced every 20 days to ensure the relatively stable solution concentration.

## 3 Test Procedures

### 3.1 Compressive Strength Test

The sulfate erosion could cause severe structural degradation and reduce the strength of the concrete. Thus, a SHT4106

**Fig. 2** Schematic diagram of sample preparation procedures



**Fig. 3** Apparatus of compressive strength test

computer-controlling electro-hydraulic serve universal testing machine was employed to test the compressive strengths of the samples immersed for 0 day, 60 days, 120 days, and 150 days (Fig. 3). The compressive strength and elasticity modulus test were conducted according to the standards GB/T 50,081–2002 and ASTM C1116-02 [45, 46]. The test was adopted force control, and the loading rate was 0.3 MPa/s. There were three samples in each group, calculating the errors between the compressive strength value of three samples and the mean value of compressive strength. If one error of them exceeded  $\pm 15\%$ , the corresponding sample will be eliminated and the mean value will be recalculated. If two errors of them exceeded  $\pm 15\%$ , this group of tests were discarded and resampled for testing. In order to overall evaluate the effect of sulfate erosion on the compressive strength, the coefficient of residual compressive strength for fiber-reinforced concrete was defined as,

$$K_f = \frac{F_t}{F_0} \quad (1)$$

where  $K_f$  is the coefficient of residual compressive strength,  $F_t$  denotes the compressive strength of sample at the sulfate erosion duration  $t$ , and  $F_0$  is the compressive strength of sample without sulfate erosion.

The relative elasticity modulus for FRC was defined as

$$R_{Ed} = \frac{E_t}{E_0} \quad (2)$$

where  $R_{Ed}$  is the relative elasticity modulus,  $E_t$  denotes the elasticity modulus of sample at the sulfate erosion duration  $t$ , and  $E_0$  is the elasticity modulus of sample without sulfate erosion.

### 3.2 Mass Change Test

The mass change could quantitatively reflects the sulfate erosion degree on concrete. The concrete samples were taken

from the solution and gently wiped the surfaces of sample to remove water and crumbs, and then the samples were weighed and recorded. The precision of the mass value is 0.01 g. The mass change was measured using the compressive strength samples for 150 days, where the final mass change was the average value of the three samples. The mass change of the group samples was tested at the intervals of 15 days. The mass change was calculated by the following:

$$\Delta m_t = \frac{m_t - m_0}{m_0} \quad (3)$$

where  $\Delta m_t$  is the mass change rate of the sample,  $m_t$  is the mass of sample at the sulfate erosion duration  $t$ , and  $m_0$  denotes the mass of sample before sulfate erosion.

### 3.3 Scanning Electron Microscope (SEM) Analysis

Paste-aggregate interface of cement motors was collected from the samples for compressive strength test at 150 days of sulfate erosion, used for SEM analysis. Firstly, the collected samples were dried in a vacuum drying oven at 60 °C for 24 h, and then the samples were sprayed with gold. Finally, FEI Inspect F50 (SEM) was used to observe its microstructure.

## 4 Results and Discussion

### 4.1 Compressive Strength Analysis

The compressive strength values of concrete samples exposed to different sulfate solution concentrations (i.e., 3%, 5%, 7% and 10%) are shown in Fig. 4 and Table 5. It can be seen that the overall performance of concrete samples added polypropylene fiber (PP1, PP2, PP4 and PP6) has been superior over those added steel fiber (SF1, SF2 and SF4) and basalt fiber (BF0.5, BF1.0, BF1.5 and BF2.0), especially for the concrete samples named PP1 and PP2. For the concrete samples PP1 and PP2, the compressive strengths increase with the erosion time. For example, after the sulfate erosion of 150 days, the compressive strengths of PP1 exposed to the sodium sulfate solution concentrations of 3%, 5%, 7% and 10% are 61.9 MPa, 61.7 MPa, 57.5 MPa and 58.3 MPa, respectively. These are 25.1%, 41.5%, 50.5% and 25.1% higher than those for the controlled concrete sample (OPC). Meanwhile, for the concrete sample PP2, the compressive strengths after the 150 days of sulfate erosion are 59.5 MPa, 57.3 MPa, 58.5 MPa and 59.6 MPa, respectively, being 20.2%, 31.4%, 53.1% and 27.9% higher than those for the OPC (Fig. 4). Figure 4 also reveals that the addition of PPF and SF could improve the compressive strength of concrete samples without the sulfate erosion (seen from the black bar chart of 0 day in Fig. 4). On the other hand,

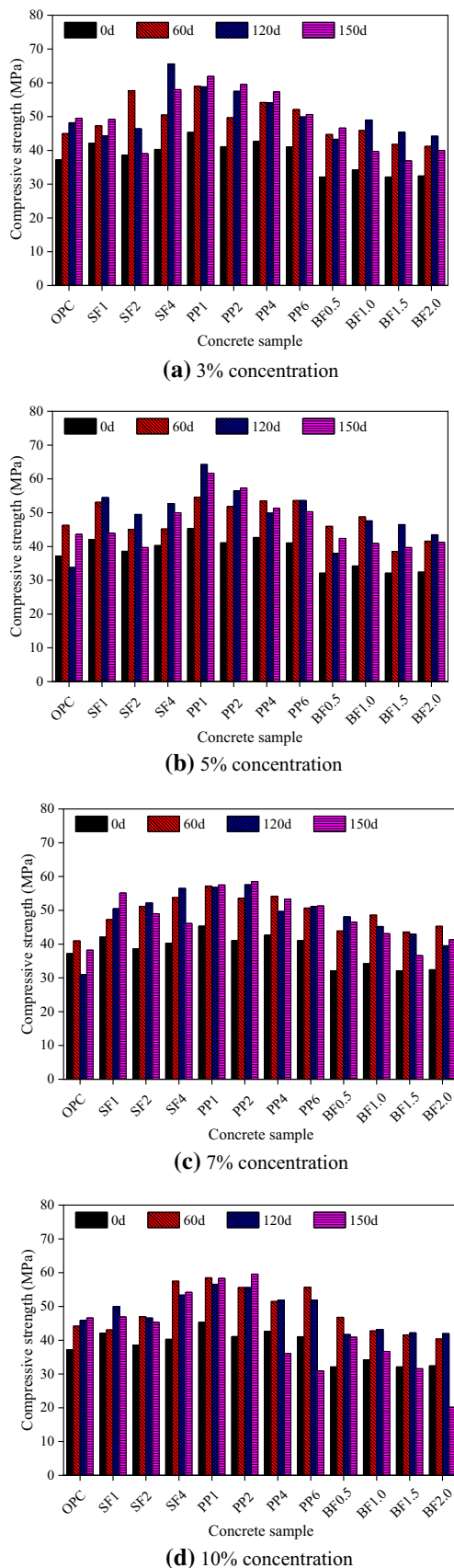


**Fig. 4** Compressive strength of concrete samples exposed to different sulfate solution concentrations

for the concrete samples added basalt fiber (i.e., BF0.5, BF1.0, BF1.5 and BF2.0), the enhancement effect of compressive strength is not obvious, which might be due to the agglomeration phenomenon of BF in concrete, resulting in the growth of internal pores and the decline of compressive strength.

Generally, as the age increased, the compressive strength would improve. So, the compressive strength of concrete exposed to sulfate erosion is the synergistic influence of age and sulfate erosion. Figure 4 indicates that the compressive strengths of all concrete samples have improved within the first 60 days erosion, and the compressive strengths of some concrete samples (e.g., OPC) are still growing in the last 90 days erosion, though the ascending rate is obviously small (Fig. 4). This is because in the later stage of erosion, the expansion force generated by the internal reactants causes the surface to fall off and the strength decreases. But at the same time, the reactants in the interior increase, filling the pores and making the internal structure denser. Additionally, the concentration of sodium sulfate solution has also affected the compressive strength of concrete samples, with the compressive strength decreases with the increase in erosion concentration (Fig. 4).

Figures 5, 6, 7 and 8 present the coefficients of residual compressive strength ( $K_f$ ) of concrete samples exposed to 3%, 5%, 7% and 10% sulfate solution concentrations, respectively. The  $K_f$  could directly determine whether the added fiber have enhancement effect on concrete. In detail, if  $K_f > 1$ , the added fibers have a positive effect on concrete; otherwise, the fiber would have a negative effect on concrete. Figures 5, 6, 7 and 8 reveal that the  $K_f$  firstly decreases and then increases with the added SF for SFRC exposed to 3%, 5% and 10% sulfate solution concentrations, and always increases for the SFRC exposed to 7% sulfate solution concentration. For the PPFRC and BFRC, the  $K_f$  has quickly increased and then gradually dropped with the added fibers except for the concrete samples after 150 days of erosion at a 10% sulfate solution concentration (Figs. 5, 6, 7 and 8). These findings suggest that, for the fiber-reinforced concrete, there is an optimum fiber content for the compressive strength of concrete samples to resist loads. It can be deduced that the optimum fiber contents for the SFRC, PPFRC, and BFRC are 3% (SF3), 1.0‰ (PP1), and 0.5‰ (BF0.5), respectively.

Generally, when the fiber content is within the appropriate range, the randomly distributed fiber bundles restrict the transverse deformation of concrete under compression. When the concrete samples are subject to load, and the fiber are bound in the matrix, the stress expands along the aggregate interface and transferred to the fiber positions, then the fiber will bear parts of load. At this time, the fibers are pulled out, the friction between the fiber and aggregate would consume a certain amount of energy, which will delay

**Table 5** Compressive strength values of all samples (MPa)

Samples	3% concentration				5% concentration				7% concentration				10% concentration			
	0 d	60 d	120 d	150 d	0 d	60 d	120 d	150 d	0 d	60 d	120 d	150 d	0 d	60 d	120 d	150 d
OPC	37.2	45	48.2	49.5	37.2	46.3	33.8	43.6	37.19	41	31	38.2	37.19	44.2	45.9	46.6
SF1	42.11	47.3	44.3	49.2	42.1	53.1	54.5	43.9	42.11	47.3	50.5	55.1	42.11	43.1	50.0	46.9
SF2	38.58	57.7	46.4	39	38.6	45.1	49.5	39.7	38.58	51.2	52.2	49	38.58	47.0	46.6	45.3
SF4	40.28	50.5	65.6	58.0	40.3	45.2	52.7	50	40.28	53.8	56.5	46.1	40.28	57.5	53.4	54.2
PP1	45.32	59	58.8	61.9	45.3	54.6	64.3	61.7	45.32	57.2	56.8	57.5	45.32	58.5	56.6	58.3
PP2	41.11	49.7	57.5	59.5	41.1	51.9	56.5	57.3	41.11	53.6	57.6	58.5	41.11	55.6	55.6	59.6
PP4	42.69	54.2	54.1	57.3	42.7	53.5	49.9	51.3	42.69	54.2	49.7	53.3	42.69	51.5	51.9	36.1
PP6	41.06	52.1	49.9	50.6	41.1	53.6	53.6	50.3	41.06	50.7	51.2	51.3	41.06	55.7	51.9	30.9
BF0.5	32.13	44.7	43.3	46.6	32.1	46	38	42.4	32.13	43.9	48.1	46.5	32.13	46.8	41.7	40.9
BF1.0	34.23	45.9	49	39.7	34.2	48.8	47.6	40.9	34.23	48.6	45.2	43.1	34.23	42.8	43.2	36.7
BF1.5	32.12	41.8	45.4	36.9	32.1	38.5	46.5	39.7	32.12	43.6	43	36.6	32.12	41.6	42.2	31.6
BF2.0	32.44	41.2	44.2	40.0	32.4	41.6	43.5	41.2	32.44	45.3	39.5	41.3	32.44	40.4	42.0	20.2

the destruction of concrete samples. Hence, the compressive strength of concrete would increase [10]. Conversely, if the fiber content exceeds the appropriate range, the surface area of fiber will drastically rise, then the negative processes of reinforcing effect could be divided into two aspects. Initially, with the total surface area of fibers increasing, more cement is required to wrap the fibers, which weakens the bonds between the cement pastes and aggregates. On the other hand, the fiber spacing in the matrix will significantly decrease due to the excessive fibers. If the fiber spacing is below a certain value, then the crossover and overlap of fibers occur, which would impact the bonds between fibers and cement pastes. Thus, some weak zones might be formed. As such, the compressive strength of concrete would drop. It is concluded that the appropriate range of fiber content should be absolutely determined in the construction design.

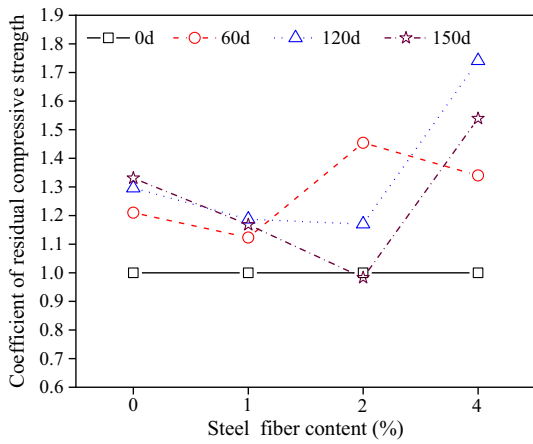
Figures 5, 6, 7 and 8 also indicate that compared with the SFRC, the PPFRC and BFRC have exhibited better resistance to sodium sulfate solution erosion at the concentrations of 3%, 5% and 7%, especially for the concrete samples PP1 with a polypropylene fiber content of 1.0‰ and BF0.5 with a basalt fiber content of 0.5‰. However, for the sulfate erosion at the concentration of 10%, the  $K_f$  is lower than zero for the concrete samples exposed to 150 days of sulfate erosion, i.e., those with the polypropylene fiber contents of 4.0‰ (PP4) and 6.0‰ (PP6), and with the basalt fiber contents of 3% (BF4) and 4% (BF4) (Fig. 8b and c). It means that the compressive strengths have drastically decreased for the four concrete samples after a 150 days of sodium sulfate solution erosion at a 10% concentration. It also indicates that the high fiber content (i.e., mainly PPF and BF) and the high sulfate

erosion concentration have a significantly negative effect on the concrete exposed to sulfate erosion.

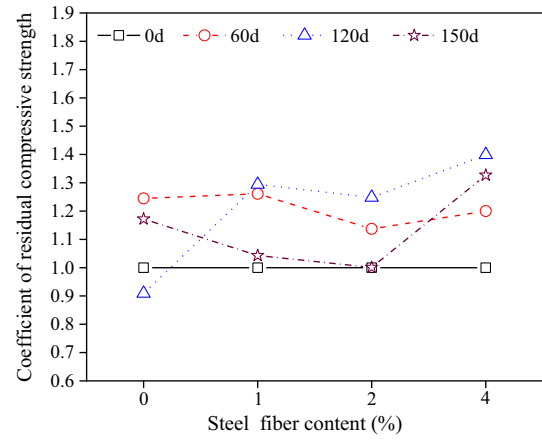
## 4.2 Resistance to Sulfate Erosion

Mass change and relative elasticity modulus could quantitatively reflect the evolution process of sulfate erosion. Figures 9 and 10 are the mass change rate and relative elasticity modulus of concrete samples exposed to sulfate solution, respectively. Generally, the mass change rates for the PPFRC have been lower than those for the BFRC, while being higher than those for the SFRC (Fig. 9). It also found that the change rates of relative elasticity modulus for PPFRC are lower than those for the BFRC (Fig. 10). For the PPFRC samples (i.e., PP1, PP2, PP4 and PP6) exposed to sulfate erosion concentrations of 3%, 5% and 7%, the mass change rate can be divided into three stages (Figs. 9 and 11). In the first stage (from 0 to 15 d), the mass change rate diminished and was lower than zero, suggesting that the PPFRC is mass losing. This might be from the fact that the sodium sulfate solution corroded the mortar on the concrete surface, and simultaneously polypropylene fibers in concrete restrain the surface crack propagation, leading to the reduction of mass, and some small cracks occur on the surface of the samples (Fig. 11a). As the erosion continued, the erosion process went into the second stage (from 15 to 135 d), whereby the mass change rate continually increased, with the pores of samples being filled by crystalline sulfate and some sulfate erosion products, leading to the growth of mass. In this stage, some crystalline sulfates and many cracks can be obviously observed on the surface of the concrete samples (Fig. 11b). In the third stage (from 135 to 150 d), with further formation of expansive products due

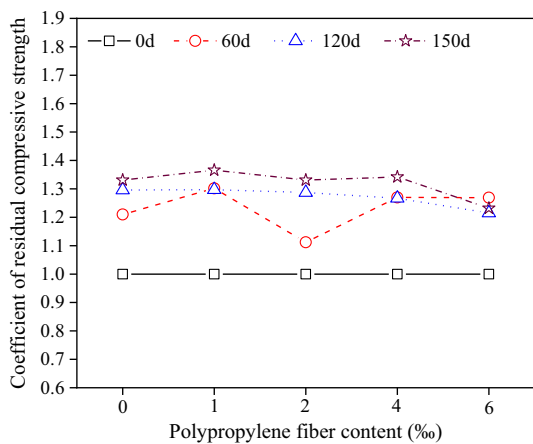




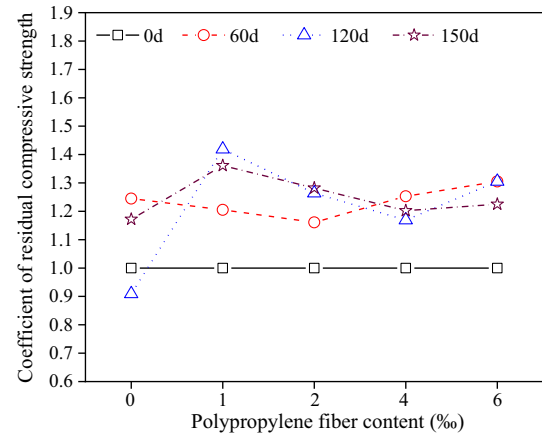
(a) SFRC



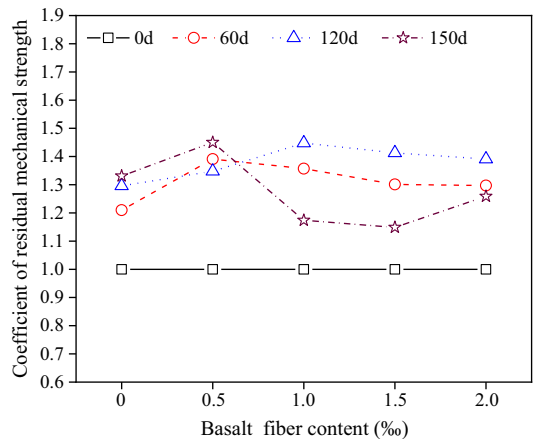
(a) SFRC



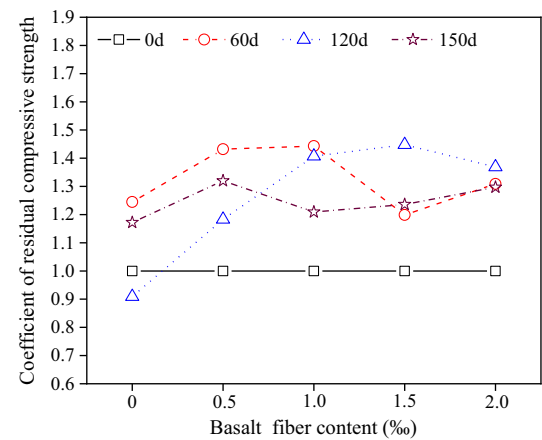
(b) PPFRC



(b) PPFRC



(c) BFRC

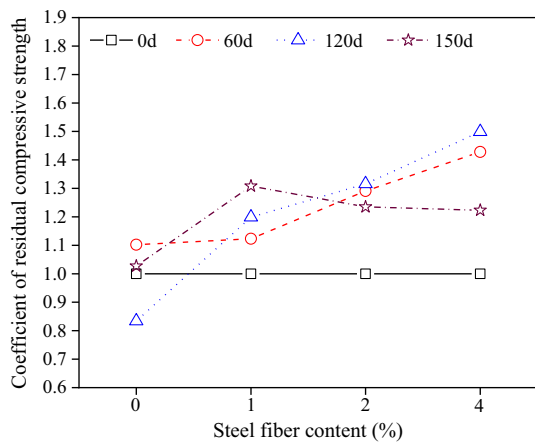


(c) BFRC

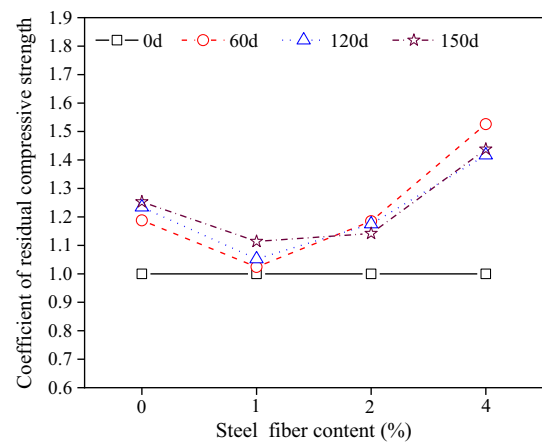
Fig. 5 Coefficient of residual compressive strength of concrete samples exposed to 3% sulfate solution concentration

Fig. 6 Coefficient of residual compressive strength of concrete samples exposed to 5% sulfate solution concentration

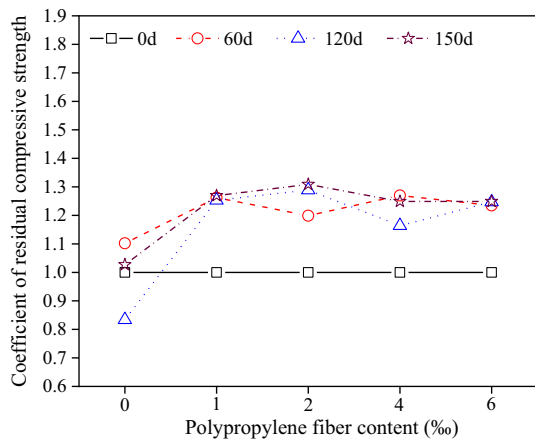




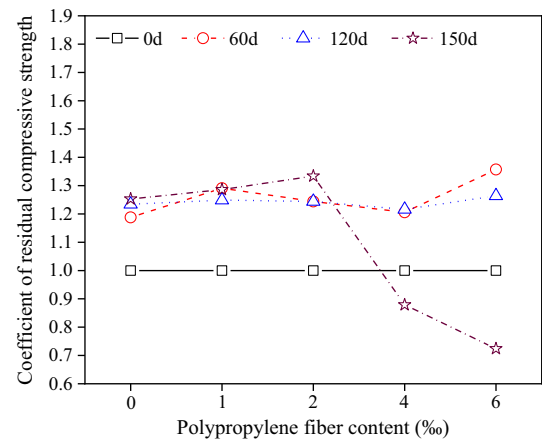
(a) SFRC



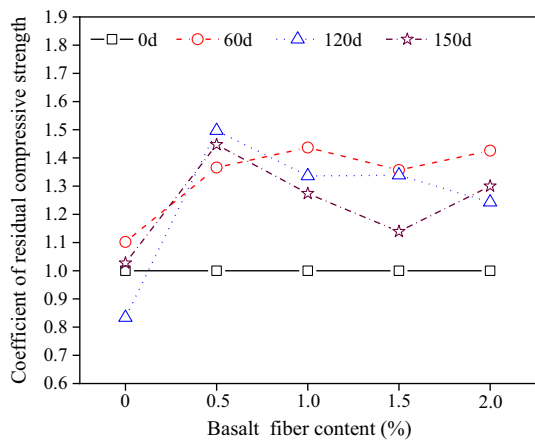
(a) SFRC



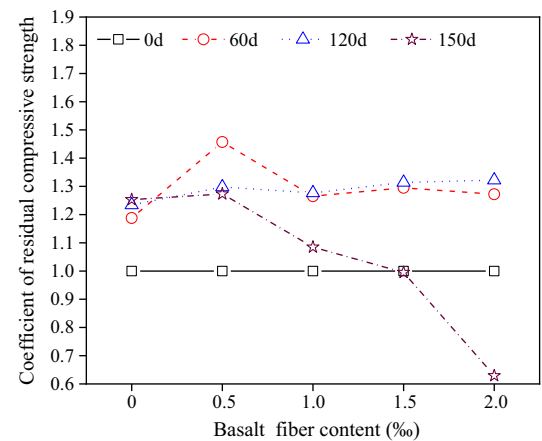
(b) PPFRC



(b) PPFRC



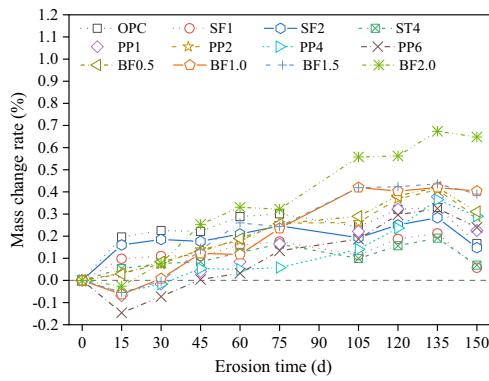
(c) BFRC



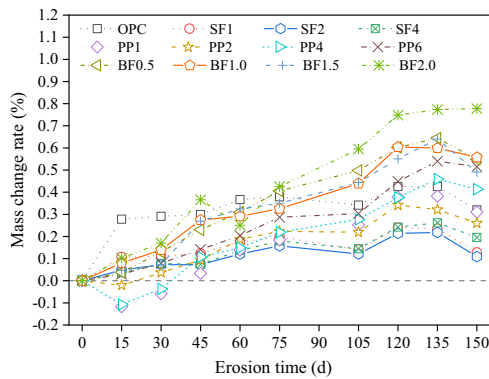
(c) BFRC

Fig. 7 Coefficient of residual compressive strength of concrete samples exposed to 7% sulfate solution concentration

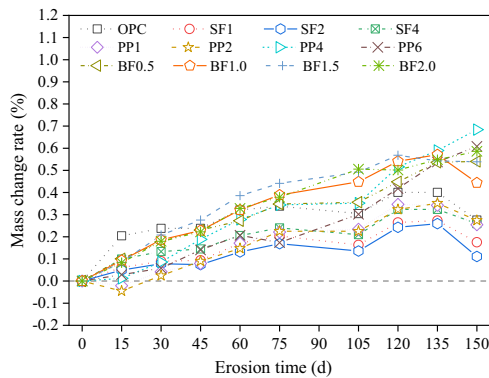
Fig. 8 Coefficient of residual compressive strength of concrete samples exposed to 10% sulfate solution concentration



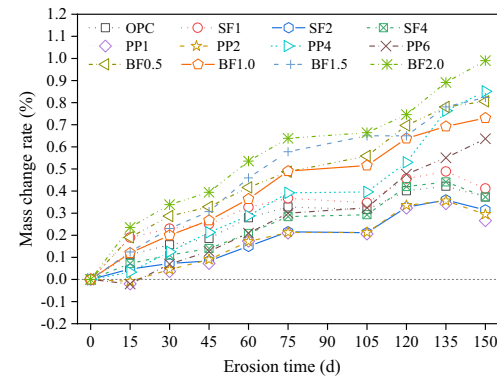
(a) 3% concentration



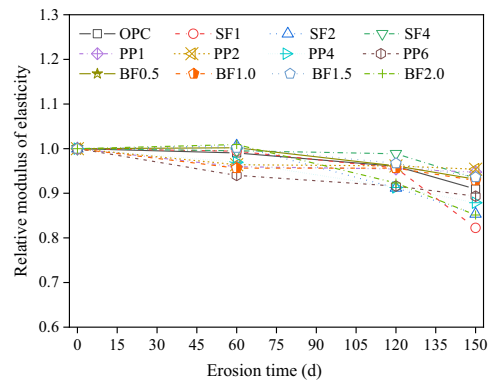
(b) 5% concentration



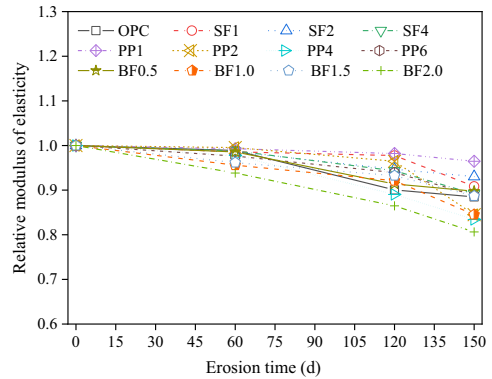
(c) 7% concentration



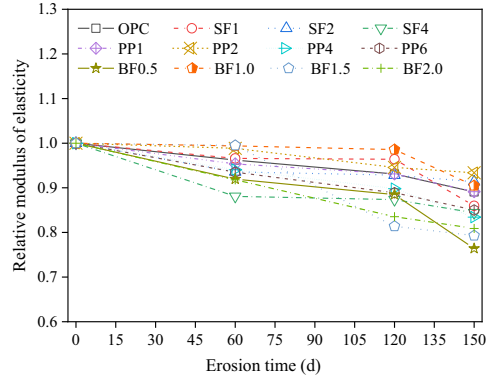
(d) 10% concentration



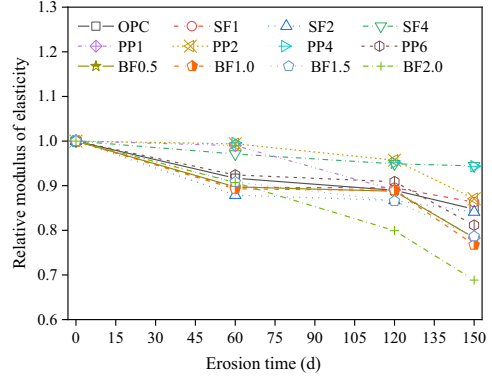
(a) 3% concentration



(b) 5% concentration



(c) 7% concentration



(d) 10% concentration

**Fig. 9** Mass change rate of concrete samples exposed to different concentrations of sodium sulfate solution

**Fig. 10** Change of the relative modulus of elasticity exposed to different concentrations of sodium sulfate solution

to the infiltration of more sulfate, resulting into the cracks in concrete matrix and peeling of mortar (Fig. 11c), and thus the mass of concrete samples is losing (Fig. 9a–c). However, for the PPFRC exposed to sulfate erosion concentration of 10%, the mass loss in the first stage is not obvious, indicating that the high concentration of sodium sulfate solution has a strong erosion on concrete (Fig. 9d). Further, the final mass change rate of concrete samples exposed to different concentrations also shows that the high concentration has a greater impact on the sulfate erosion of concrete samples (Fig. 9). These findings are in line with the analysis of compressive strength analysis (Figs. 5, 6, 7, 8). Figure 9 also illustrates that the variation trends of mass change rates for the SFRC are closer than those for the controlled group (OPC), and the electrochemical corrosion occurs during the sulfate erosion varying from 0 to 135 d, leading to steel corrosion and slight mass loss. At the late erosion stage (from 135 to 150 d), the mass change rates for the SFRC have drastically decreased, and it might be from the fact that the expansion products in the interface bond zone are easier to fall off due to the hydrophobicity of SF, reducing the adhesion between the steel fibers and matrix (Fig. 9). Additionally, for the BFRC, the mass change rate has grown as the fiber contents increased, especially for the BF2.0 (Fig. 9).

From Fig. 10, it can be seen that the relative elasticity modulus decreases with the erosion time increased (Fig. 10). The variation of relative elasticity modulus can be divided into two stages. In detail, in the first stage (from 0 to 120 d), the relative elasticity modulus slowly decreases, because the sulfate corrosion is not serious at this stage, and salt crystals are mostly formed on the surface of concrete. In the second stage (from 120 to 150 d), the relative elasticity modulus rapidly decreases. In this stage, the sulfate enters into the interior of concrete through the cracks generated by salt crystallization and reacts with hydration products. Thus, more cracks occurred and the relative elasticity modulus reduced. Besides, it also shows that the concentration of sodium sulfate solution has a significant influence on the relative elasticity modulus of concrete, and the relative elasticity modulus decreases with the concentrations of sodium sulfate solution for the same sulfate erosion period (Fig. 10).

### 4.3 SEM Analysis

To further explore the erosion process of sodium sulfate solution on FRC, the microstructure of OPC, SFRC (SF1), PPFRC (PP4), and BFRC (BF2.0) exposed to different concentrations of sodium sulfate solution was obtained. Figure 12 is the SEM images of OPC exposed to different concentrations of sodium sulfate solution after 150 days. It can be seen that the OPC structure without sulfate erosion is complete, the cement matrix is compact, and there

are only a few initial micro-cracks on the surface of structure (Fig. 12a). After 150 days of sulfate erosion in a 5% sodium sulfate solution, some prismatic crystals (gypsum) and needle-like crystals (ettringite) could be observed in the OPC, which might lead to the crystallization pressure on the pore structure (Fig. 12a). Further, for the concentration of sodium sulfate solution (10%), the number and shape of ettringite has increased and accumulated to form clusters, whereby more cracks are clearly observed in the OPC (Fig. 12). These observations indicate that the sulfate erosions have a significant influence on the structure of OPC.

Figures 13, 14 and 15 are the SEM images of SFRC with SF content of 1.0%, PPFRC with PPF content of 4.0%, and BFRC with BF content of 2.0% exposed to different concentrations of sodium sulfate solution after 150 days, respectively. The path of SF can be clearly observed, indicating that the SF was pulled out in SFRC and the bond between the SF and concrete matrix was weak (Fig. 13a). However, the PPF and the hardened cement matrix were tightly bonded though there are some micro-pores in PPFRC, indicating that the PPF has good fiber-matrix binding quality in PPFRC compared to the SF (Fig. 14a). Besides, some initial cracks in BFRC without sulfate erosion were observed, which might be caused by the calcium silicate hydrate gel (C-S-H) due to the hydration reaction (Fig. 15a). The expansion products, mainly salt crystallization, gypsum and ettringite, are formed in the concrete exposed to sulfate erosion, and the number and shape also increased with the erosion age and sulfate solution concentration, along with the depth and width of cracks in concrete (Figs. 12, 13, 14 and 15). Generally, sulfate erosion on the concrete matrix is characterized by the reaction of sulfate ions with cement hydration products, which would lead to expansion, cracking and even spalling, as well as strength loss and mass change [47]. The sulfate erosion on concrete has a dual effect on the performance of concrete. This because the gypsum and ettringite, which are the two main products in sulfate erosion, have positive and negative influence on concrete. Both chemical sulfate erosion and physical sulfate erosion simultaneously occur. With the sulfate erosion duration, some expansion products, e.g., salt crystallization, gypsum and ettringite would form, leading to expand solid volume and higher crystallization pressure. Thus, the microstructures in concrete surface are growing. On the other hand, the sulfate solution infiltrates into the pores in structure and react with the hydration products, then forming more expansion products accompanied with expansion. When the expansion occurs, because of the small diameter of fiber and short distance between fibers, especially for the PPF, the path of crack tips would be limited due to the existence of fibers. Thus, the cracks could only move by passing the fiber, pulling out the fiber, or even breaking the fiber. The fiber fracture and fiber pullout must consume massive external energy.

**Fig. 11** Three stages of PPFRC exposed to sulfate erosion concentration of 5%

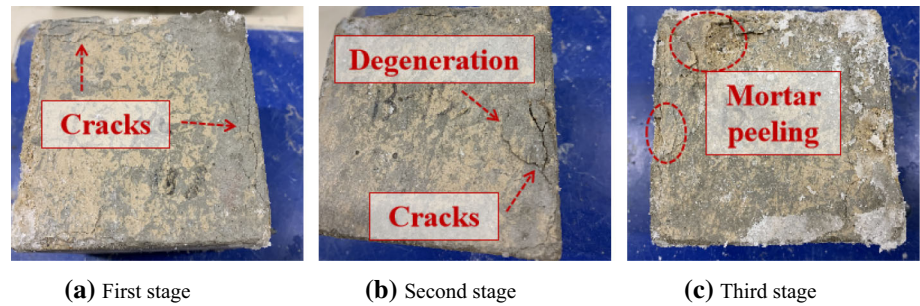
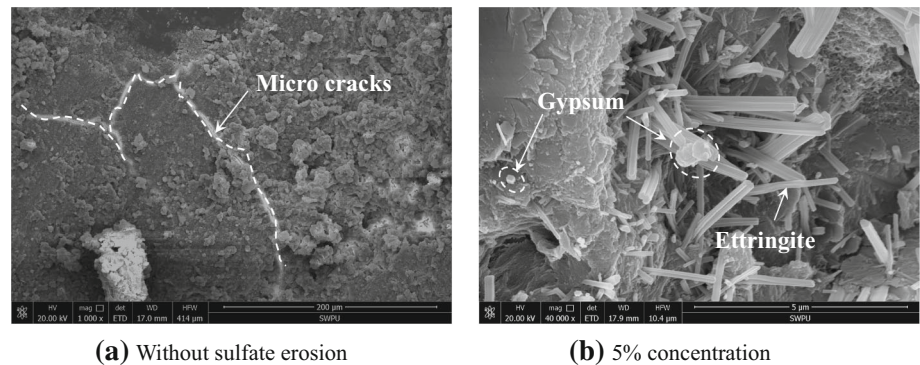


**Fig. 12** SEM images of OPC exposed to different concentrations of sodium sulfate solution after 150 days



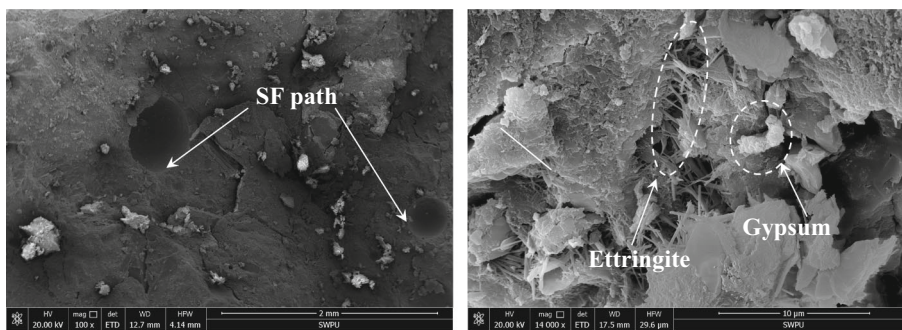
Thus, the compressive strengths of fiber-reinforced concrete, especially for the PPFRC, would increase.

## 5 Conclusions

This study investigated the mechanical properties and microstructure of SFRC, PPFRC and BFRC exposed to sulfate erosion based on a series of experiments. Some conclusions are obtained as follows.

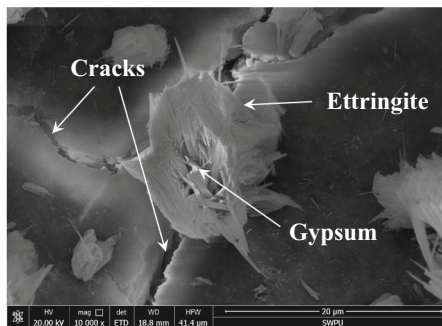
- (1) The addition of PPF and SF could improve the compressive strength of concrete without sulfate erosion, while for the concrete added BF, the enhancement effect of compressive strength was not obvious, which might be due to the agglomeration phenomenon of BF in concrete, resulting in growth of internal pores and the reduction of compressive strength.
- (2) The concentration of sodium sulfate solution affected the compressive strength and relative elasticity modulus of concrete, the compressive strength and relative elasticity modulus diminished as the erosion concentration increased. For the FRC, there was an optimum fiber content for the compressive strength of concrete samples to resist sulfate erosion, and the optimum fiber contents for the SFRC, PPFRC and BFRC were 3.0%, 1.0% and 0.5%, respectively.
- (3) The mass change rates for the PPFRC were lower than those for the BFRC, while being higher than those for the SFRC. For the PPFRC exposed to sulfate erosion concentrations of 3%, 5% and 7%, the mass change rate could be divided into three stages, i.e., declining stage with the mass change rate below zero, increasing stage with the pores of concretes filling by some expansion products and diminishing stage with some mortar peeling out. For the BFRC, the mass change rate

**Fig. 13** SEM images of SFRC with SF content of 1.0% exposed to different concentrations of sodium sulfate solution after 150 days



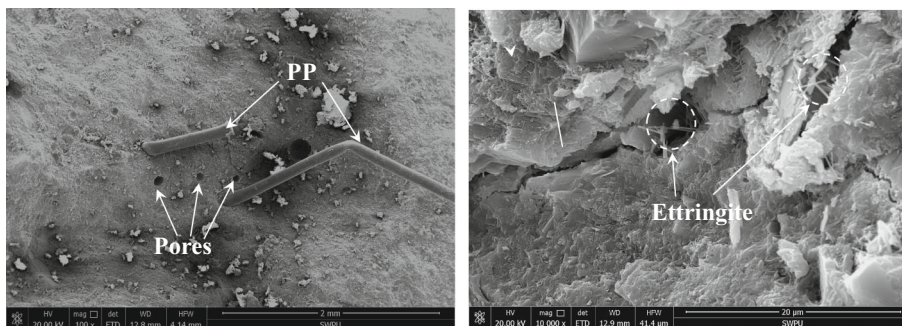
(a) Without sulfate erosion

(b) 5% concentration



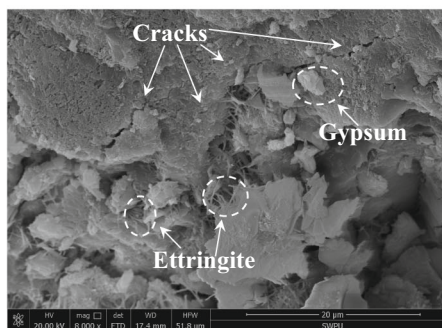
(c) 10% concentration

**Fig. 14** SEM images of PPFRC with PPF content of 4.0% exposed to different concentrations of sodium sulfate solution after 150 days



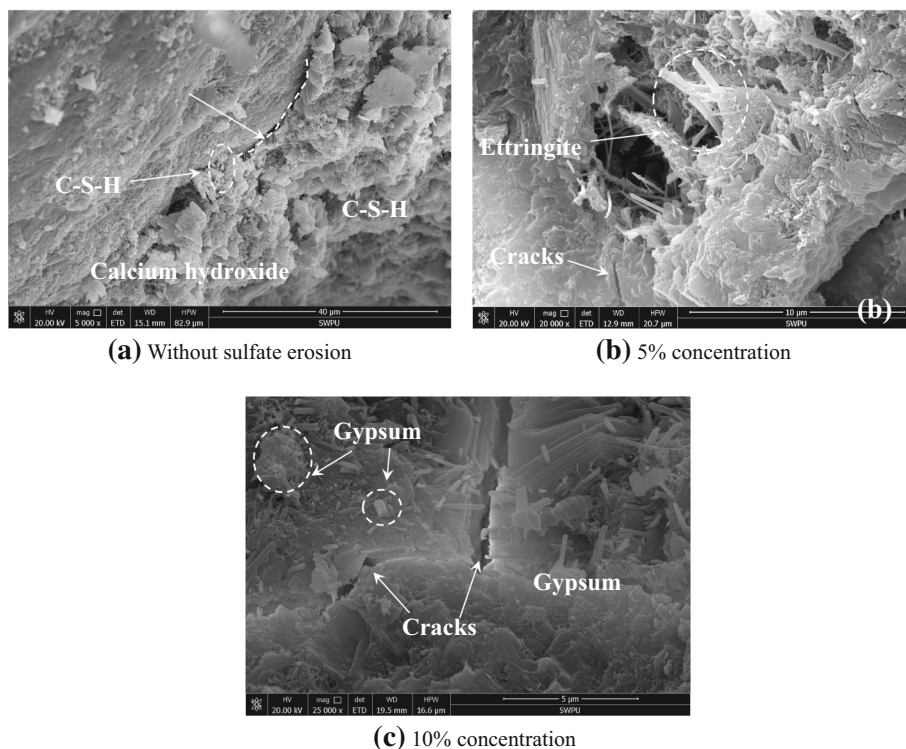
(a) Without sulfate erosion

(b) 5% concentration



(c) 10% concentration

**Fig. 15** SEM images of BFRC with BF content of 2.0% exposed to different concentrations of sodium sulfate solution after 150 days



increases with the fiber contents increased, especially for the BF2.0.

- (4) Compared to the SF and BF, the PPF had a good fiber-matrix binding quality in PPFRC. The number and shape of expansion products, e.g., salt crystallization, gypsum and ettringite, increased with the erosion age and sulfate solution concentration increased, together with the depth and width of cracks in concrete.

**Funding** This research was supported by the National Natural Science Foundation of China (Grant Nos. 42101136, 42071087), the China Postdoctoral Science Foundation (Grant No. 2021M692697), the State Key Laboratory of Frozen Soil Engineering (Grant No. SKLFSE202007), the Sichuan Science and Technology Program (Grant No. 2021YFQ0021), and the Sichuan Youth Science and Technology Innovation Research Team (Grant No. 2019JDTD0017).

**Conflict of interest** The authors declare that they have no conflict of interest.

## References

- Uygunoğlu, T.: Investigation of microstructure and flexural behavior of steel-fiber reinforced concrete. *Mater. Struct.* **41**(8), 1441–1449 (2008)
- Yin, S.; Tuladhar, R.; Shi, F.; Combe, M.; Collister, T.; Sivakugan, N.: Use of macro plastic fibres in concrete: a review. *Constr. Build. Mater.* **93**, 180–188 (2015)
- Pakravan, H.R.; Ozbakkaloglu, T.: Synthetic fibers for cementitious composites: a critical and in-depth review of recent advances. *Constr. Build. Mater.* **207**, 491–518 (2019)
- Wei, B.; Cao, H.; Song, S.: Tensile behavior contrast of basalt and glass fibers after chemical treatment. *Mater. Des.* **31**(9), 4244–4250 (2010)
- Wei, B.; Cao, H.; Song, S.: Degradation of basalt fibre and glass fibre/epoxy resin composites in seawater. *Corros. Sci.* **53**(1), 426–431 (2011)
- Sun, J.; Ding, Z.; Li, X.; Wang, Z.: Bond behavior between BFRP bar and basalt fiber reinforced seawater sea-sand recycled aggregate concrete. *Constr. Build. Mater.* **285**, 122951 (2021)
- Fiore, V.; Di Bella, G.; Valenza, A.: Glass–basalt/epoxy hybrid composites for marine applications. *Mater. Des.* **32**(4), 2091–2099 (2011)
- Sim, J.; Park, C.; Moon, D.Y.: Characteristics of basalt fiber as a strengthening material for concrete structures. *Compos. B Eng.* **36**(6–7), 504–512 (2005)
- Borhan, T.M.: Properties of glass concrete reinforced with short basalt fibre. *Mater. Des.* **42**, 265–271 (2012)
- Niu, D.; Su, L.; Luo, Y.; Huang, D.; Luo, D.: Experimental study on mechanical properties and durability of basalt fiber reinforced coral aggregate concrete. *Constr. Build. Mater.* **237**, 117628 (2020)
- Fallah, S.; Nematzadeh, M.: Mechanical properties and durability of high-strength concrete containing macro-polymeric and polypropylene fibers with nano-silica and silica fume. *Constr. Build. Mater.* **132**, 170–187 (2017)
- Cao, S.; Yilmaz, E.; Song, W.: Fiber type effect on strength, toughness and microstructure of early age cemented tailings backfill. *Constr. Build. Mater.* **223**, 44–54 (2019)



13. Katkhuda, H.; Shatarat, N.: Improving the mechanical properties of recycled concrete aggregate using chopped basalt fibers and acid treatment. *Constr. Build. Mater.* **140**, 328–335 (2017)
14. Afroughsabet, V.; Biolzi, L.; Ozbakkaloglu, T.: High-performance fiber-reinforced concrete: a review. *J. Mater. Sci.* **51**(14), 6517–6551 (2016)
15. Song, P.S.; Hwang, S.: Mechanical properties of high-strength steel fiber-reinforced concrete. *Constr. Build. Mater.* **18**(9), 669–673 (2004)
16. Köksal, F.; Altun, F.; Yiğit, İ.; Şahin, Y.: Combined effect of silica fume and steel fiber on the mechanical properties of high strength concretes. *Constr. Build. Mater.* **22**(8), 1874–1880 (2008)
17. Tassew, S.T.; Lubell, A.S.: Mechanical properties of glass fiber reinforced ceramic concrete. *Constr. Build. Mater.* **51**, 215–224 (2014)
18. Al-Ameeri, A.: The effect of steel fiber on some mechanical properties of self-compacting concrete. *Am. J. Civ. Eng.* **1**(3), 102 (2013)
19. Giner, V.T.; Baeza, F.J.; Ivorra, S.; Zornoza, E.; Galao, Ó.: Effect of steel and carbon fiber additions on the dynamic properties of concrete containing silica fume. *Mater. Des.* **34**, 332–339 (2012)
20. Hsu, L.S.; Hsu, C.T.T.: Stress–strain behavior of steel-fiber high-strength concrete under compression. *ACI Struct. J.* **91**(4), 448–457 (1994)
21. Libre, N.A.; Shekarchi, M.; Mahoutian, M.; Soroushian, P.: Mechanical properties of hybrid fiber reinforced lightweight aggregate concrete made with natural pumice. *Constr. Build. Mater.* **25**(5), 2458–2464 (2011)
22. Bissonnette, B.; Pigeon, M.: Tensile creep at early ages of ordinary, silica fume and fiber reinforced concretes. *Cem. Concr. Res.* **25**(5), 1075–1085 (1995)
23. García-Taengua, E.; Arango, S.; Martí-Vargas, J.R.; Serna, P.: Flexural creep of steel fiber reinforced concrete in the cracked state. *Constr. Build. Mater.* **65**, 321–329 (2014)
24. Cheung, A.K.F.; Leung, C.K.Y.: Shrinkage reduction of high strength fiber reinforced cementitious composites (HSFRCC) with various water-to-binder ratios. *Cement Concr. Compos.* **33**(6), 661–667 (2011)
25. Güneyisi, E.; Gesoğlu, M.; Mohamadameen, A.; Alzebaree, R.; Algin, Z.; Mermerdaş, K.: Enhancement of shrinkage behavior of lightweight aggregate concretes by shrinkage reducing admixture and fiber reinforcement. *Constr. Build. Mater.* **54**, 91–98 (2014)
26. Yuan, Z.; Jia, Y.: Mechanical properties and microstructure of glass fiber and polypropylene fiber reinforced concrete: An experimental study. *Constr. Build. Mater.* **266**, 121048 (2021)
27. Dong, J.F.; Wang, Q.Y.; Guan, Z.W.: Material properties of basalt fibre reinforced concrete made with recycled earthquake waste. *Constr. Build. Mater.* **130**, 241–251 (2017)
28. Wan, X.; Gong, F.; Qu, M.; Qiu, E.; Zhong, C.: Experimental study of the salt transfer in a cold sodium sulfate soil. *KSCE J. Civ. Eng.* **23**(4), 1573–1585 (2019)
29. Wan, X.; Hu, Q.; Liao, M.: Salt crystallization in cold sulfate saline soil. *Cold Reg. Sci. Technol.* **137**, 36–47 (2017)
30. Yang, J.S.: Development and prospect of the research on salt affected soils in China. *Acta Pedol. Sin.* **45**(5), 837–845 (2008)
31. Yu, C.; Sun, W.; Scrivener, K.: Degradation mechanism of slag blended mortars immersed in sodium sulfate solution. *Cem. Concr. Res.* **72**, 37–47 (2015)
32. Al-Dulaijan, S.U.: Sulfate resistance of plain and blended cements exposed to magnesium sulfate solutions. *Constr. Build. Mater.* **21**(8), 1792–1802 (2007)
33. Hossack, A.M.; Thomas, M.D.A.: The effect of temperature on the rate of sulfate attack of Portland cement blended mortars in Na<sub>2</sub>SO<sub>4</sub> solution. *Cem. Concr. Res.* **73**, 136–142 (2015)
34. Liu, Z.; De Schutter, G.; Deng, D.; Yu, Z.: Micro-analysis of the role of interfacial transition zone in “salt weathering” on concrete. *Constr. Build. Mater.* **24**(11), 2052–2059 (2010)
35. Gao, J.; Yu, Z.; Song, L.; Wang, T.; Wei, S.: Durability of concrete exposed to sulfate attack under flexural loading and drying–wetting cycles. *Constr. Build. Mater.* **39**, 33–38 (2013)
36. Ehlert, R.A.: Coral concrete at bikini atoll. *Concr. Int.* **13**, 19–24 (1991)
37. Zhao, K.; Qiao, Y.; Zhang, P.; Bao, J.; Tian, Y.: Experimental and numerical study on chloride transport in cement mortar during drying process. *Constr. Build. Mater.* **258**, 119655 (2020)
38. Han, S.; Zhong, J.; Yu, Q.; Yan, L.; Ou, J.: Sulfate resistance of eco-friendly and sulfate-resistant concrete using seawater sea-sand and high-ferrite Portland cement. *Constr. Build. Mater.* **305**, 124753 (2021)
39. Santhanama, M.; Cohenb, M.D.; Olek, J.: Mechanism of sulfate attack: a fresh look: Part 2 Proposed mechanisms. *Cem. Concr. Res.* **33**(3), 341–346 (2003)
40. Lee, S.T.; Moon, H.Y.; Swamy, R.N.: Sulfate attack and role of silica fume in resisting strength loss. *Cem. Concr. Compos.* **27**(1), 65–76 (2005)
41. Huang, D.; Niu, D.; Su, L.; Fu, Q.: Chloride diffusion behavior of coral aggregate concrete under drying–wetting cycles. *Constr. Build. Mater.* **270**, 121485 (2021)
42. Wang, J.; Niu, D.: Influence of freeze–thaw cycles and sulfate corrosion resistance on shotcrete with and without steel fiber. *Constr. Build. Mater.* **122**, 628–636 (2016)
43. Ben, X.; Jiang, L.; Guo, M.Z.; Meng, Y.; Chen, L.; Jin, W.; Wang, F.: Chloride erosion resistance of calcium format incorporated cement mortar under chloride attack. *Constr. Build. Mater.* **314**, 125611 (2022)
44. He, R.; Zheng, S.; Gan, V.J.L.; Wang, Z.; Fang, J.; Shao, Y.: Damage mechanism and interfacial transition zone characteristics of concrete under sulfate erosion and dry–wet cycles. *Constr. Build. Mater.* **255**, 119340 (2020)
45. CS (Chinese Standard) GB/T 50081–2002 standard for test method of mechanical properties on ordinary concrete (in Chinese)
46. Standard specification for fiber-reinforced concrete and shot concrete (ASTM C1116-02). Philadelphia, P. A.: American Society for Testing and Materials (ASTM)
47. Wee, T.H.; Suryavanshi, A.K.; Wong, S.F.; AnisurRahman, K.M.: Sulfate resistance of concrete containing mineral admixtures. *ACI Mater. J.* **97**(5), 536–549 (2000)
48. Al-Amoudi, O.S.B.: Attack on plain and blended cements exposed to aggressive sulfate environments. *Cem. Concr. Compos.* **24**(3–4), 305–316 (2002)

